Adaptive Variable Impedance Control for Multi-axis Force Tracking in Uncertain Environment Stiffness with Redundancy Exploitation

Muhammad Bilal * **Muhammad Nadeem Akram** **
Mohsin Rizwan *

* *Human-Centered Robotics Lab, Al-Khwarizmi Institute of Computer Science, National Center of Robotics and Automation, University of Engineering & Technology, Lahore-54890, Pakistan (e-mail: muhammad.bilal@kics.edu.pk; mohsin.rizwan@uet.edu.pk).*
** *Department of Mechanical, Automotive, and Materials Engineering, University of Windsor, Windsor, Ontario, Canada (e-mail: akram113@uwindsor.ca)*

Abstract: This paper presents an adaptive variable impedance control methodology for force tracking on multi-axis robotic activity in uncertain environmental stiffness along with redundancy exploitation. The classical force control schemes are not effective for force tracking in uncertain environments; therefore, a revised impedance control scheme is proposed herein. The mathematical model of the robot's motion, including its kinematics and dynamics, alongside the proposed control scheme has been discussed in detail. The robotic system's redundancy is exploited to avoid singularities. A series of simulations based on the practical scenarios have been carried out on a 3R planar robot considering the uncertain environmental stiffness. The results indicate that the proposed control approach significantly reduces the force-error-overshoot during the transition in environmental stiffness. Besides, the manipulability index is reasonably improved as well.

Keywords: Position based impedance control, force tracking, uncertain environment stiffness, adaptive variable impedance control, redundancy resolution

1. INTRODUCTION

Incorporation of sophisticated force control strategies among an industrial robot is crucial to its performance while carrying out a demanding industrial task within an uncertain environment e.g., grinding, polishing, assembling, surface cleaning, etc. The interaction between the robot's end-effector and the environment is presented as shown in Fig. 1. For such applications, a motion control strategy is not enough to execute a contact-based operation accurately. The contact operation can be effectively executed using the motion control strategies provided the mathematical model of the robot, as well as, the environment model is completely known. In most cases, the mathematical model of the robot can be calculated with a higher degree of accuracy Siciliano and Villani (2000); Spong et al. (2004), but the environmental model cannot be formulated with much high precision. Due to an inaccurate and incomplete model, force error may cause an actuator to reach a saturation point, or even cause some damage to the mechanical part under construction. If the robot model and the environmental parameters are estimated accurately, the stated drawbacks can be overcome. Due to uncertainty in model parameters, force tracking is one of the primary challenges for the precise execution of contact-based tasks. Besides, a robot's inability to execute the required tasks near singular regions must be addressed. In the case of a redundant manipulator, the extra degree of freedom (DOF) is utilized for singularity avoidance Yoshikawa (1984) Maciejewski and Klein (1985) Yahya et al. (2012).

Over the last two decades, force tracking remains the main concern of the researchers. Initially, force tracking

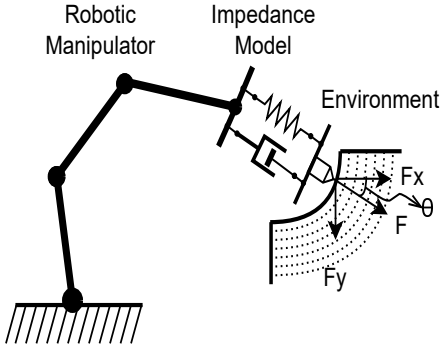

Fig. 1. Robot-Environment force interaction: In case of impedance control, the robot's end-effector behaves as mass-spring-damper system as presented. The force component is divided into x and y axis based on angle θ.

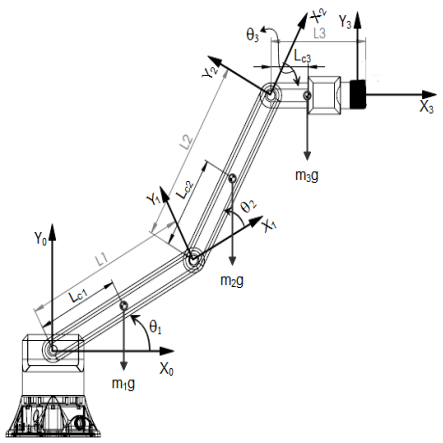

Fig. 2. Schematic model of the 3R planar robot: The complete list of the parameters, including link lengths, joint variables, frame of references, center of link lengths, center of gravity of each link, are presented on 3R planar robot. These parameters are used for deriving the kinematics and dynamics formulations.

control was implemented using two fundamental force control schemes: 1) Hybrid position and force control Craig (1981), and 2) Impedance control Hogan (1985). During the contact-based operation within a static environment, these force control schemes provide satisfactory performance with an accurate estimation of the environmental parameters. On the contrary, the schemes has been failed in converging the steady-state force error to zero within a dynamically changing environment Jinjun et al. (2018); Lu and Meng (1991). To resolve this issue, multiple control strategies have been proposed to handle the force tracking in an uncertain environment to handle contact-based operation. Early literature proposed two control schemes to generate the reference position trajectory, irrespective of a known environment. In the first case, a direct adaptive control scheme was implemented to generate the on-line reference position based on the force tracking error. In the second case, indirect adaptive control scheme was used to estimate the environmental parameters, and henceforth to compute the reference position trajectory Seraji (1997). A model reference adaptive control scheme (MRAC) used the force tracking error to generate the reference position trajectory Seraji (1997). The extended Kalman filter was used to estimate the parameters to generate a precise reference trajectory as per the desired force dynamics Deng et al. (2016). To incorporate the actual geometry of the environment, the contact, shape, and surface normal of the environment were estimated Wang et al. (2016). For an uncertain environment, a position-based impedance control scheme was implemented using adaptive control to effectively track the desired force Zhang and Khamesee (2017). The nonlinear model-based variable impedance parameters controller (MVIPC) was proposed for hydraulic drive unit Ba et al. (2020). However, the MVIPC has not incorporated the adaptation mechanism as well as not dealt with the uncertain environmental stiffness. The intelligent force control techniques were proposed to compensate for the environmental uncertainty using the neural networks Jung and Hsia (2000) and fuzzy-neural schemes Kiguchi and Fukuda (2000). In all the above-mentioned control schemes, the force tracking is reliant upon the estimated environmental parameters, thereby making the force tracking faulty. Besides, no dynamic relationship exists between the robot's end-effector and its operating environment.

To cater to the mentioned drawbacks, an impedance control scheme was employed considering an uncertain environment stiffness. The reference trajectory was generated based on the force tracking error, and the robust position control was implemented to compensate for the uncertainty in the robot dynamics Jung et al. (2001). The advantages of implementing a variable impedance control scheme for the execution of the task are studied in Kronander and Billard (2012); Buchli et al. (2011). The stability of variable impedance control was studied and a state-independent stability constraint was proposed to relate the damping effect to stiffness and its derivative Kronander and Billard (2016). The stability and overall efficiency of the variable impedance control scheme were improved by incorporating the redundancy resolution Ficuciello et al. (2015). Recent studies have addressed the problem of changing impedance specification through reinforcement learning Buchli et al. (2011); Roy et al. (2013), and online based learning by varying impedance stiffness Kronander and Billard (2012); Calinon et al. (2010); Abu-dakka et al. (2018). To handle the uncertainties and external disturbances, a fuzzy adaptive hybrid impedance-based control was proposed Xianjun and Xi (2018). However, learning-based approaches demand exhaustive initial training of the system and are not suitable for force tracking. The adaptive variable impedance control law was proposed to minimize the force error on single axis without redundancy exploitation Jinjun et al. (2018). For multi-axis force tracking activity with redundancy exploitation, the revised adaptive variable impedance control scheme is presented in details. Moreover, the realistic parameters are employed to check the effectiveness of the revised adaptive variable impedance control scheme as well as considered multiple differ scenarios for simulations to validate it.

In summary, this research work proposes a control scheme for multi-axis force tracking in uncertain environment stiffness while exploiting the redundancy resolution to keep the configuration of the robotic manipulator away from the singular configuration. To the best of our knowledge, in open literature, no work has been done in the past to evaluate the performance of multi-axis force tracking while avoiding singularity. The rest of the paper is arranged as follows. Robot kinematics and dynamics are discussed in section 2. In section 3, robot control schemes, stability and convergence of proposed approach are explained. A simulation studies are discussed in section 4 followed by conclusion in section 5.

2. ROBOT MODELING

In this section, the kinematics and dynamics formulations of a redundant robot have been described in detail. Kinematics deals with the relationship between the end-effector or tool pose (position and orientation) and the joint variables. Whereas, the robot dynamics deals with the relationship between joint accelerations and joint torques.

2.1 Kinematics

Using forward position kinematics, the relationship between the joint space variables and the task space variables is expressed as

$$x = f(\theta) \tag{1}$$

By taking the derivative of equation (1) w.r.t time, the following equation is obtained

$$\dot{x} = J\dot{\theta} \tag{2}$$

where J depicts the Jacobian matrix, which refers the joints velocities with the task space velocities. In terms of a non-redundant manipulator, the Jacobian matrix will be of full rank and provides a unique solution. To compute the joint velocities for the given end-effector velocities, equation (2) becomes

$$\dot{\theta} = J^{-1}\dot{x} \tag{3}$$

In the context of a redundant manipulator, the non-squared Jacobian matrix loses rank and provides multiple solutions to achieve the desired end-effector pose. There are two common methods available for solving the inverse of a non-squared Jacobian matrix: 1) Moore-Penrose pseudo-inverse method and 2) Damped-least square (DLS) method. Moore-Penrose pseudo-inverse method Albert (1972) provides solution with the minimum norm joint velocities. Mathematically represented as

$$\dot{\theta} = J^{+}\dot{x} \tag{4}$$

where $J^{+} = J^{T}(JJ^{T})^{-1}$ is termed as a right pseudo-inverse of J. The general solution of equation (4) is expressed as

$$\dot{\theta} = J^{+}\dot{x} + (I - J^{+}J)z \tag{5}$$

where I and z represent the identity matrix and arbitrary vector in $\dot{\theta}$ space, respectively. The second term in equation (5) corresponds to the self-motion of the joints and does not change the end-effector position. In the context of a DLS method Wampler (1986), the J^{+} is mathematically represented as

$$J^{+} = J^{T}(JJ^{T} + \lambda^{2}I)^{-1} \tag{6}$$

where λ represent the damping factor and can be expressed as Chiaverini et al. (1991)

$$\lambda^{2} = \begin{cases} 0, & \text{if } \sigma_m \geq \kappa \\ \left(1 - \left(\frac{\sigma_m}{\kappa}\right)^{2}\right)\lambda_m^{2}, & \text{otherwise} \end{cases} \tag{7}$$

where σ_m depicts the maximum singular value, κ represents the singular region size and λ_m indicates the maximum damping factor value.

2.2 Redundancy Resolution

Redundancy resolution is the procedure of choosing the best possible solution among the infinite solutions. The term $(I - J^{+}J)z$ also known as an optimization term or homogeneous solution of the Jacobian matrix and can be used to optimize the desired objective function $\Omega(\theta)$. Multiple techniques are available to avoid the singularity occurrence. One technique used for avoiding the singularity is the gradient projection method Wan et al. (2018). By taking

$$z = \mu\nabla\Omega(\theta) \tag{8}$$

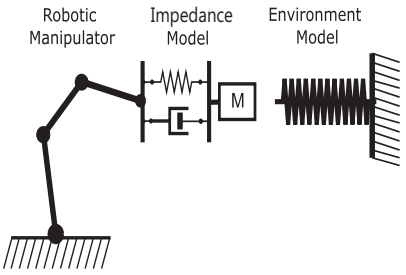

(a) End-effector approaching to environment

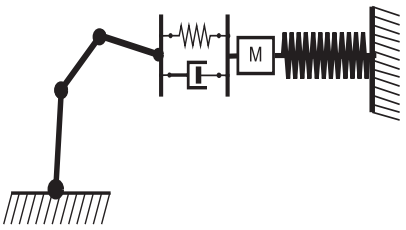

(b) Initial contact phase

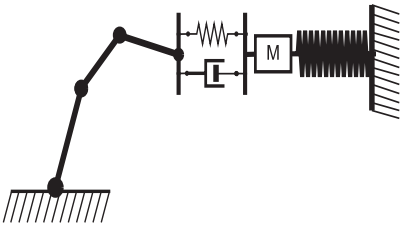

(c) End-effector exerting desired force on the environment

Fig. 3. Interaction between the robot's end-effector and the environment: The environment model is represented by the spring element while impedance model is represented by mass-spring-damper system.

where ∇ and μ represent the gradient of the objective function $\Omega(\theta)$ and trade-off between the optimization and the minimization of $\Omega(\theta)$, respectively. By using equation (8) into (5), the following equation is derived

$$\dot{\theta} = J^{+}\dot{x} + \mu(I - J^{+}J)\nabla\Omega(\theta) \tag{9}$$

where $\nabla\Omega(\theta)$ is,

$$\nabla\Omega(\theta) = \begin{pmatrix} \frac{\partial\Omega}{\partial\theta_1} & \cdots & \frac{\partial\Omega}{\partial\theta_n} \end{pmatrix} \tag{10}$$

Another technique proposed by Yoshikawa Yoshikawa (1985), to avoid the singular configurations is more simple and stable. According to Yoshikawa Yoshikawa (1985), the performance criteria is $P = \sqrt{det\ (JJ^{T})}$. Thus, equation (9) is modified to

$$\dot{\theta} = J^{+}\dot{x} + (I - J^{+}J)zk \tag{11}$$

where z and k are expressed as

$$z = \frac{1}{2}\sqrt{detG}\sum_{i,j=1}^{m}\left[G^{-1}\right]_{ij}\left({}_{q}J_i'J_j^{\intercal} + {}_{q}J_j'J_i^{\intercal}\right)$$

$$k = \frac{k_1}{2\left(\sqrt{z(I - J^{+}J)z^{\intercal}}\right)}, \quad 0 \leq k_1 \leq 1$$

where,

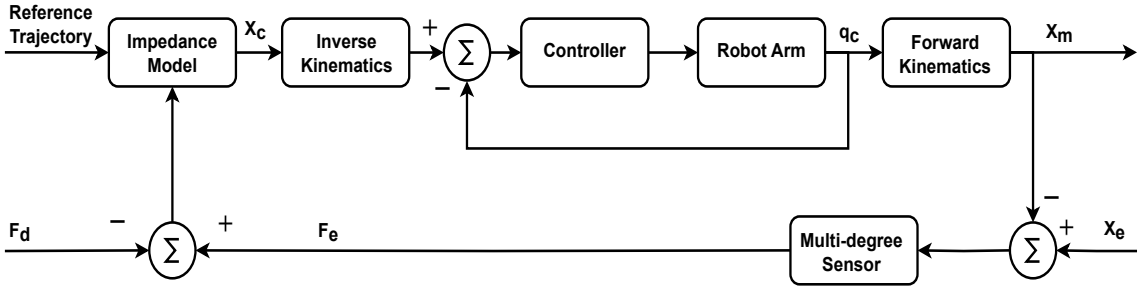

Fig. 4. Block diagram of position-based impedance control law for force tracking: The reference trajectory along with the net force computes the commanded position followed by inverse kinematics calculation. The PID controller is used to control the robot arm. Moreover, a multi-degree sensor is used to get the force data.

$$\begin{aligned} G &= JJ^{\intercal} \quad where \quad i,j = 1,2,\cdots,m \\ \left[G^{-1}\right]_{ij} &= i,j \ element \ of \ G^{-1} \\ J_i &= i^{th} \ row \ of J \\ {}_qJ_i' &= derivative \ of \ J_i \ w.r.t \ \theta_q \end{aligned}$$

2.3 Robot Dynamics

Forward dynamics computes the joint accelerations for the given joint torques. On the other hand, the inverse dynamics provides joint torques for the given joint accelerations. To derive the closed-form equation of motion, Newton-Euler formulation results in the equations involving the constraint forces, and, explicit expressions for joint torques expression cannot be derived. On the contrary, the Euler-Lagrange formulation represents the motion of the system in terms of the energy and work instead of force and momentum. Using Euler-Lagrange formulation, the equation of motion in joint space is expressed as

$$\frac{d}{dt}\left(\frac{\partial K}{\partial \dot{q}}\right) - \frac{\partial K}{\partial q} = H\ddot{q} + \dot{H}\dot{q} - \begin{bmatrix} \dot{q}^T \dfrac{\partial H}{\partial q_1}\dot{q} \\ \vdots \\ \dot{q}^T \dfrac{\partial H}{\partial q_n}\dot{q} \end{bmatrix} = H\ddot{q} + V(q,\dot{q}) \tag{12}$$

$$H(q)\ddot{q} + C(q,\dot{q})\dot{q} + g(q) + f(\dot{q}) = \tau - J^T F_{ext} \tag{13}$$

where,

$q, \dot{q}, \ddot{q}$	=	Joint position, velocity, and acceleration
$H(q)$	=	Positive-definite inertial matrix
$g(q)$	=	Gravitational forces
$f(\dot{q})$	=	Frictional forces
$C(q,\dot{q})\dot{q}$	=	Coriolis and centrifugal terms
J	=	Jacobian matrix
F_{ext}	=	External forces on end-effector
τ	=	Joint torques

The schematic model of the 3R planar robot is shown in Fig. 2. Where m, L, and L_c represent link mass, link length, and center of link length, respectively.
In the contact space, where robot's end-effector interacts with the environment, it is appropriate to depict the equation of motion in task space. Equation of motion for 3R planar robot in task space can be represented as

$$H_x(x)\ddot{x} + C_x(x,\dot{x})\dot{x} + g_x(x) + f_x(\dot{x}) = J^{-T}\tau - F_{ext} \tag{14}$$

where,

$$\begin{aligned} H_x &= J^{-T} H J^{-1} \\ C_x(x,\dot{x}) &= J^{-T}(C - HJ^{-1}\dot{J})J^{-1} \\ g_x &= J^{-T} g \\ f_x(\dot{x}) &= J^{-T} f \end{aligned} \tag{15}$$

3. ROBOT CONTROL

Impedance behavior can be depicted by a mass-spring-damper system. For the given reference trajectory, impedance relationship is represented as

$$M_d(\ddot{X} - \ddot{X}_r) + B_d(\dot{X} - \dot{X}_r) + K_d(X - X_r) = -F_{ext}(t) \tag{16}$$

$$M_d(\ddot{E}) + B_d(\dot{E}) + K_d(E) = -F_{ext}(t) \tag{17}$$

where M_d, B_d, and K_d represent the desired inertia, damping, and stiffness, respectively. Whereas, X, X_r, and F_{ext} express the virtual position, desired position, and applied force (measured by the force sensor mounted on the end-effector), respectively.

3.1 Position-based Impedance Control for Force Tracking

The schematic model of the contact between the robot's end-effector and the environment are shown in Fig. 3. The robot's end-effector is represented by the mass-spring-damper system while the environment is characterized by the stiffness k_e. In the first phase, the robot's end-effector is approaching the environment followed by the initial contact in the second phase. In the third phase, the robot's end-effector is exerting the desired force on the environment.
The general block diagram of position based impedance control law (PBICL) for force tracking is shown in Fig. 4. The reference trajectory X_r along with the force error $\Delta F = F_e - F_d$ compute the commanded trajectory X_c. Where F_e and F_d represent the actual force and desired force, respectively. The commanded joint position is calculated using the inverse kinematics followed by the servo drive system. The actual position X_m of the end-effector is computed using the forward position kinematics.
During contact operation, the position error is expressed as

$$E = X_m - X_r = X_c - X_r \tag{18}$$

The contact force F_e between the environment and the robot's end-effector is

$$F_e = K_e(X_e - X_m) = K_e(X_e - X_c) \tag{19}$$

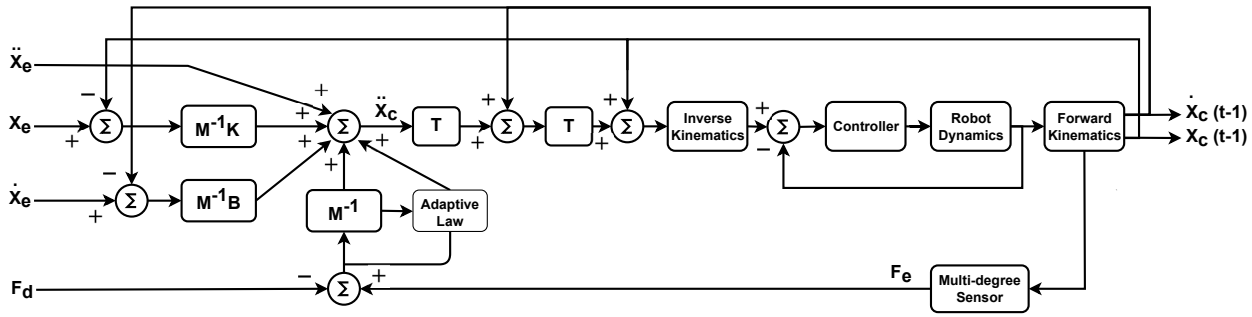

Fig. 5. Block diagram of adaptive variable impedance control scheme: The adaptive law used trajectory difference with necessary multiplication to compute the commanded position followed by inverse kinematics computation. After that, the same inner loop has been implemented as Fig. 3

where X_e represents the environment position. The dynamic relationship between the force error ΔF and the position perturbation E is

$$M\frac{d^2E(t)}{dt^2} + B\frac{dE(t)}{dt} + KE(t) = \Delta F(t) \tag{20}$$

To modify the reference trajectory, the position perturbation E is utilized to compute the commanded position X_c as

$$X_c = X_r + E = X_r + \Delta F \cdot K(s) \tag{21}$$

where $K(s)$ represent the mass-spring-damper system as

$$K(s) = \frac{1}{ms^2 + bs + k} \tag{22}$$

During contact operation, consider 1 DOF system to derive the expression for the reference trajectory. The force error is expressed as

$$\Delta f = f_e - f_d = k_e(x_e - x_c) - f_d = k_e x_e - k_e(x_r + k(s)\Delta f) - f_d \tag{23}$$

By substituting the relation equation (22) in (23), the following expression is obtained

$$\Delta f(ms^2 + bs + k + k_e) = (ms^2 + bs + k)[k_e(x_e - x_r) - f_d] \tag{24}$$

Using equation (24), the steady-state force error is represented as

$$\Delta f_{ss} = \frac{k}{k + k_e}[k_e(x_e - x_r) - f_d] \tag{25}$$

To ensure the convergence of steady-state force error to zero, the reference trajectory should be computed according to the following expression

$$x_r = x_e - \frac{f_d}{k_e} \tag{26}$$

In order to compute the reference trajectory equation ((26)), all the parameters f_d, x_e, and k_e must be known. In practical scenarios, it is complex to determine the environment's stiffness and location. Hence, classical PBICL is not suitable to effectively execute the contact operation. To efficiently complete the tasks, the existing approach needs to be modified. In the case of uncertain environment stiffness, it is difficult to compute the reference trajectory as equation (26). By replacing $e = x_c - x_r$ and $\Delta f = f_e - f_d$ in equation (20) gives

$$f_e - f_d = m(\ddot{x}_c - \ddot{x}_r) + b(\dot{x}_c - \dot{x}_r) + k(x_c - x_r) \tag{27}$$

By swapping x_r with x_e returns

$$f_e - f_d = m(\ddot{x}_c - \ddot{x}_e) + b(\dot{x}_c - \dot{x}_e) + k(x_c - x_e) \tag{28}$$

Consider two cases for evaluating the uncertain environment stiffness. In the first scenario, the robot's end-effector merely contact with the environment $f_d = 0$. Equation (28) always valid for the first case. In the second case, the robot's end-effector employed desired force $f_d \neq 0$ on the environment. As a result, the $x_c \neq x_e$ yields $\Delta f_{ss} \neq 0$. In order to converge the steady-state force error to zero, the target stiffness k should be zero for an uncertain environment stiffness and location Jung et al. (2004).

3.2 Adaptive Variable Impedance Control Scheme

In the previous section, it is observed that the desired stiffness should be zero for the convergence of steady-state force error to zero. Let consider two cases, the first case is the free-space control where the end-effector is approaching the environment. In the second case, the end-effector is in contact with the environment and termed as contact-space control. Considering the first case, equation (28) becomes

$$-f_d = m(\ddot{e}) + b(\dot{e}) + k(e) \tag{29}$$

where $e = x_e - x$, the term f_d represents the driving force that exerts by the robot's end-effector on the environment. In the contact-space with the uncertain environment stiffness, the condition $k = 0$ satisfy the steady-state requirement of f_e=f_d. During contact-space, equation (28) becomes

$$f_e - f_d = m(\ddot{e}) + b(\dot{e}) \tag{30}$$

As a result, the target stiffness is kept zero during the contact-space, whereas, non-zero stiffness value is considered in free-space. Thus, the proposed control scheme is simple, robust, and stable for force tracking problems under uncertain environmental stiffness. Consider a practical case, the uncertain environment position x'_e can be written as

$$\begin{aligned} \delta x_e &= x'_e - x_e \\ e' &= e + \ \delta x_e \end{aligned} \tag{31}$$

where δx_e is the uncertainty in the environmental position. Using equation (31), the equation (29) and (30) are expressed as

$$-f_d = m(\ddot{e}'') + b(\dot{e}') + k(e') \tag{32}$$

$$f_e - f_d = m(\ddot{e}'') + b(\dot{e}') \tag{33}$$

To ensure the contact, the environment position should be always over-estimating such that $\delta x_e > 0$. Hence, the

proposed adaptive variable impedance control scheme for multi-axis can be expressed as

$$m\ddot{e}'' + b(\dot{e}' + \psi) = f_e - f_d \tag{34}$$

where ψ is modified online based on the force error,

$$\psi(t) = \psi(t-\xi) + \gamma \frac{f_d(t-\xi) - f_e(t-\xi)}{b} \tag{35}$$

The terms ξ and γ represent the sampling period and update rate of the controller, respectively. The general block diagram of adaptive variable impedance control law is shown as in Fig. 5.

3.3 Convergence and Stability of Proposed Control Law

In this section, the convergence and stability of the proposed control scheme are examined mathematically. By combining equation (34) and (35) yields

$$\begin{aligned} -(f_d(t) + \gamma f_d(t-\xi)) &= m\ddot{e}''(t) \\ &+ b\dot{e}'(t) + k_e e(t) + b\psi(t-\xi) + \gamma k_e e(t-\xi) \end{aligned} \tag{36}$$

Using the expression $f_e = k_e(x - x_e)$, the time derivatives are represented as

$$x = x_e + \frac{f_e}{k_e}, \quad \dot{x} = \dot{x}_e + \frac{\dot{f}_e}{k_e}, \quad \ddot{x} = \ddot{x}_e + \frac{\ddot{f}_e}{k_e} \tag{37}$$

Using equation (37) into (36), the following equation is obtained

$$\begin{aligned} &m(-\ddot{f}_e) + b(-\dot{f}_e) + bk_e\psi(t-\xi) + k_e(f_d - f_e) = \\ &-mk_e\delta\ddot{x}_e - bk_e\delta\dot{x}_e - \gamma k_e\left(f_d(t-\xi) - f_e(t-\xi)\right) \end{aligned} \tag{38}$$

Adding $m\ddot{f}_d$ *and* $b\dot{f}_d$ on both sides gives

$$\begin{aligned} m(\ddot{f}_d - \ddot{f}_e) + b(\dot{f}_d - \dot{f}_e) + b\psi(t-\xi) + k_e(f_d - f_e) \\ = m\ddot{f}_d + b\dot{f}_d - mk_e\delta\ddot{x}_e - bk_e\delta\dot{x}_e \\ - \gamma k_e\left(f_d(t-\xi) - f_e(t-\xi)\right) \end{aligned} \tag{39}$$

Defining $\epsilon(t) = f_d(t) - f_e(t)$, the equation (39) is reduced to

$$\begin{aligned} m\ddot{\epsilon}(t) + b\dot{\epsilon}(t) + k_e\left(\epsilon(t) + b\,\Psi(t-\xi) + \gamma\epsilon(t-\xi)\right) = \\ m\ddot{f}_d + b\dot{f}_d - mk_e\delta\ddot{x}_e - bk_e\delta\dot{x}_e \end{aligned} \tag{40}$$

Using the principle of dispersion, k elements of Ψ series can be represented as

$$\begin{aligned} b\psi(t-\xi) = b\psi\left(t-(k-1)\xi\right) + \gamma\epsilon\left(t-(k-2)\xi\right) \\ + \cdots + \gamma\epsilon(t-2\xi) \end{aligned} \tag{41}$$

Let suppose that the initial Ψ is zero such that $\psi(t-(k-1)\xi) = 0$. By combining equation (40) and (41) yields

$$\begin{aligned} m\ddot{\epsilon}(t) + b\dot{\epsilon}(t) + k_e\epsilon(t) + \gamma k_e(\epsilon(t-(k-1)\xi) \\ + \cdots + \epsilon(t-\xi)) = m\ddot{f}_d + b\dot{f}_d - m\delta\ddot{x}_e - b\delta\dot{x}_e \end{aligned} \tag{42}$$

Let $\overline{f_e} = k_e\delta x_e$, the equation (42) directs to

$$\begin{aligned} m\ddot{\epsilon}(t) + b\dot{\epsilon}(t) + k_e\epsilon(t) + \gamma k_e(\epsilon(t-(k-1)\xi) \\ + \cdots + \epsilon(t-\xi)) = m\ddot{\varepsilon} + b\dot{\varepsilon} \end{aligned} \tag{43}$$

where $\varepsilon = f_d - \overline{f}_e$, the Laplace transform of equation (43) can be written as

$$\frac{\epsilon(s)}{\varepsilon(s)} = \frac{ms^2 + bs}{\left(ms^2 + bs + k_e + k_e\gamma(e^{-(k-1)\xi s} + \cdots + e^{-\xi s})\right)} \tag{44}$$

The stability of the equation (44) can be examined by the characteristics equation as

$$\left(ms^2 + bs + k_e + k_e\gamma\left(e^{-(k-1)\xi s} + \cdots + e^{-\xi s}\right)\right) = 0 \tag{45}$$

For the given conditions, k is supposed to be a large number and expression $|e^{-\xi s}|$ should not be equal to 1, then the sum of the series can be expressed as

$$\sum_{n=1}^{\infty} e^{-\xi sn} = \frac{1}{1 - e^{-\xi s}} - 1 \tag{46}$$

By substituting equation (46) into (45) gives

$$\left(ms^2 + bs + k_e + k_e\gamma\left(\frac{e^{-\xi s}}{1 - e^{-\xi s}}\right)\right)\epsilon(s) = 0 \tag{47}$$

The term $e^{-\xi s}$ can be approximated as $e^{-\xi s} \approx 1 - \xi s$ using Taylor series expansion for high sampling period as written

$$\xi ms^3 + b\xi s^2 + k_e\xi(1-\gamma)s + k_e\gamma = 0 \tag{48}$$

To check the stability of the system, the Routh-Hurwitz stability criterion is employed as

s^3	ξm	$k_e\xi(1 - \gamma)$
s^2	$b\xi$	γk_e
s^1	c_1	0
s^0	c_0	0

where c_1 and c_0 are

$$c_1 = \frac{bk_e\xi^2(1-\gamma) - \xi\gamma mk_e}{b\xi} > 0 \tag{49}$$

$$c_0 = \gamma k_e > 0 \tag{50}$$

From equation (49), the terms m, b, and ξ should be greater than 0. The bounded region for the update rate can be represented as

$$0 < \gamma < \frac{b\xi}{b\xi + m} \tag{51}$$

The steady-state error of equation (44) is

$$E_{ss}(s) = \lim_{s\to 0} s\left(\epsilon(s) - \varepsilon(s)\right) = -1 \tag{52}$$

The following conclusion can be drawn as $t \to \infty, f_e \to f_d$

$$\lim_{t\to\infty} \epsilon(t) = 0 \tag{53}$$

4. SIMULATIONS AND RESULTS

The proposed control scheme is implemented on a 3R planar redundant robot to analyze the force tracking performance. Simulations incorporated the practical scenarios to effectively validate the proposed approach. The manipulability measure technique is adopted to represent the manipulability ellipsoids. The DLS method is employed as a primary task to resolve the inverse kinematics of the 3R planar robot along with the singularity avoidance algorithm. In order to evaluate the performance in uncertain environment stiffness, the output of the proposed scheme, for force tracking on flat surface, is compared with the classical impedance control scheme Hogan (1985). The results, as shown in Fig. 6 and 7, indicate the limitations of the classical impedance control scheme. Due to significant force error overshoot, the classical impedance control scheme is not suitable for force tracking on complex geometry profiles. A series of simulations based on the multiple industrial applications are carried out using MATLAB & SIMULINK. In order to observe real-time behavior, the simulations incorporated the full-arm dynamics along with the actual DC motor parameters. The robot's model

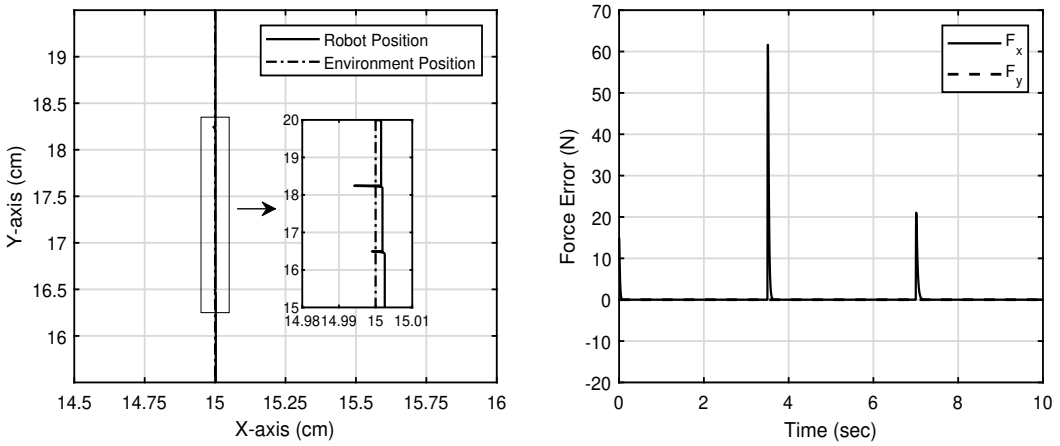

(a) Position tracking (b) Force tracking error

Fig. 6. Position and force tracking on flat surface using **classical impedance control scheme**: The position error at variation of stiffness shows small overshoot as compared to force error which amounted to $62N$ and $21N$. These error values are very large for contact tasks and may cause serious damage to part under operations.

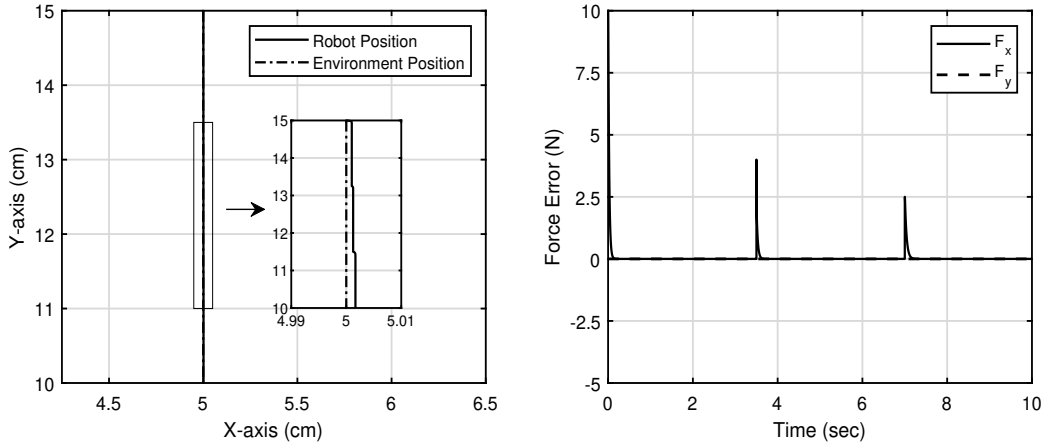

(a) Position tracking (b) Force tracking error

Fig. 7. Position and force tracking on flat surface using **adaptive variable impedance control**: The error values are significantly reduced during position and force tracking as compared to classical impedance control scheme

parameters are $m_1 = m_2 = m_3 = 0.250\ kg$, and links length are $L_1 = 22.1\ cm, L_2 = 15.6\ cm$, and $L_3 = 19.7\ cm$. Considering torque and speed requirements, Maxon DC-X $35L\ \phi 35\ mm$ motor along with $60:1$ gear head is selected for all joints. The parallel form PID controller gains are tuned using the Gradient descent method based on the Sequential Quadratic Programming algorithm. In all simulation studies, the robot's end-effector is assumed to be initially contacted with the environment.

4.1 Force Tracking on Flat Surface

The performance of the classical impedance control scheme Hogan (1985) is examined by the force tracking on a flat surface which satisfies $\dot{X}_e = \ddot{X}_e = 0$. The constant controller parameters are taken as $M = diag[1;1]$, $B = diag[200;200]$, and $K = diag[40;0]$. Due to 3R planar redundant robot, the gains along the $z-axis$ are ignored. Besides, to observe the effectiveness of a classical impedance control scheme, the stiffness of the environment is varied as

$$K_e = \begin{cases} 10000\ (N/m), & 0 \le t < 3.5 \\ 8000\ (N/m), & 3.5 \le t < 7 \\ 6000\ (N/m), & 7 \le t \le 10 \end{cases}$$

Figure 6a and 6b show the position and force tracking performance, respectively. Due to change in the environment stiffness, the force overshoots are observed at $t = 3.5\ sec$ and $7\ sec$. The classical impedance control scheme provides a reasonably well position tracking performance, whereas, the force overshoots are prominent and may cause damage to the part under operation. To resolve this issue, the revised adaptive variable impedance control scheme is implemented to effectively converge the force error to zero with minimum force error overshoot. The initial guess of the damping gains along both axes are selected as $B = diag[260;260]$ and constant $M = diag[1;1]$. The stable range of the update rate γ for the given controller parameters are:

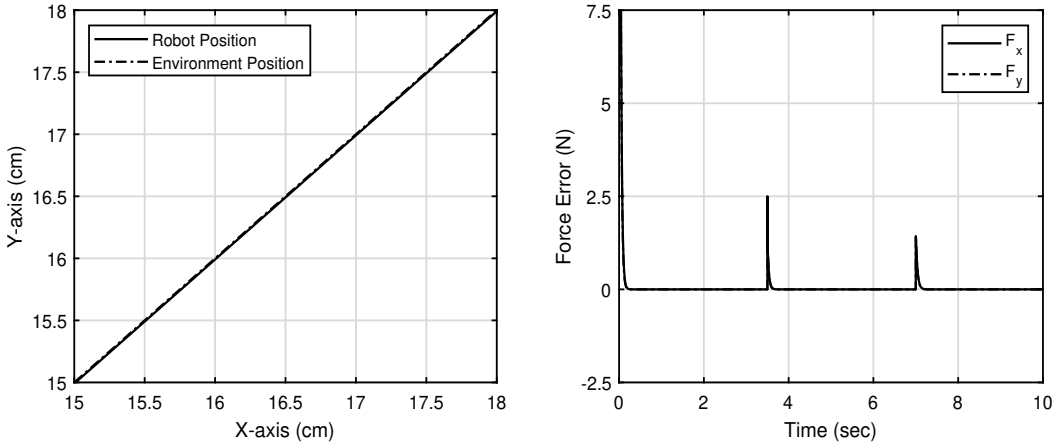

(a) Position tracking (b) Force tracking error

Fig. 8. Position and force tracking on slope surface using **adaptive variable impedance control**

Table 1. Robot's position values during force tracking on flat surface with sharp edges as well as the values of joint variables using damped-least square method with or without singularity avoidance. The higher manipulability index values depict the configuration of the manipulator far from the singular configuration.

Sr.	Robot Position		Damped-Least Square method				DLS + Singularity Avoidance			
	x (cm)	y (cm)	θ_1 (rad)	θ_2 (rad)	θ_3 (rad)	**manip index**	θ_1 (rad)	θ_2 (rad)	θ_3 (rad)	**manip index**
1	16.5	17.0	-0.85	2.16	0.39	**652.42**	-0.85	2.16	0.39	**652.42**
2	16.5	16.9	-0.86	2.17	0.39	**649.26**	-0.86	2.16	0.39	**649.75**
3	16.5	14.4	-1.00	2.20	0.45	**609.58**	-0.99	2.17	0.49	**615.43**
4	17.0	11.5	-1.18	2.22	0.51	**574.95**	-1.15	2.15	0.61	**591.97**
5	19.4	9.13	-1.29	2.17	0.52	**604.55**	-1.25	2.08	0.65	**626.45**
6	19.5	7.72	-1.37	2.18	0.54	**594.54**	-1.28	2.07	0.68	**622.78**
7	19.4	5.94	-1.47	2.18	0.58	**580.78**	-1.39	2.04	0.76	**613.56**
8	18.8	5.31	-1.52	2.19	0.61	**561.76**	-1.50	2.05	0.87	**571.33**
9	16.5	2.85	-1.74	2.22	0.74	**495.35**	-1.61	2.04	0.97	**539.02**
10	16.5	1.23	-1.83	2.21	0.77	**496.60**	-1.73	1.96	1.09	**549.23**
11	16.5	-3.32	-2.04	2.14	0.84	**519.92**	-1.89	1.81	1.22	**585.84**
12	16.5	-8.32	-2.20	2.05	0.87	**573.56**	-1.99	1.64	1.30	**643.90**
13	16.5	-13.3	-2.29	1.95	0.84	**647.46**	-2.05	1.47	1.34	**717.59**
14	16.5	-18.3	-2.33	1.84	0.77	**731.54**	-2.07	1.30	1.34	**798.45**
15	16.5	-23.3	-2.32	1.73	0.69	**815.04**	-2.05	1.12	1.31	**876.43**
16	16.5	-28.3	-2.28	1.62	0.59	**887.09**	-2.01	0.94	1.26	**940.39**
17	16.5	-32.3	-2.23	1.51	0.50	**928.63**	-1.98	0.85	1.23	**962.87**

$$0 \leq \gamma \leq \frac{0.001 \times 260}{0.001 \times 260 + 1}$$

As shown in Fig. 7b, the steady-state force error is effectively converged to zero same as for classical impedance control scheme while force error overshoot is much smaller. In addition, position tracking performance of proposed scheme is comparatively better than classical impedance control scheme as shown in Fig. 7a. Hence, the proposed control scheme surpasses the classical impedance control scheme during the force tracking on varying environment stiffness.

4.2 Force Tracking on Slope Surface

In order to evaluate the efficiency of the proposed scheme for redundant robot in 2D surface, it is implemented for force tracking on a slope surface (x and y both varying simultaneously) which satisfies $\dot{X}_e \neq 0$ *and* $\ddot{X}_e = 0$. The environment stiffness is varied as

$$K_e = \begin{cases} 8000\ (N/m), & 0 \leq t < 3.5 \\ 7000\ (N/m), & 3.5 \leq t < 7 \\ 6000\ (N/m), & 7 \leq t \leq 10 \end{cases}$$

The preliminary damping gains are taken as $B = diag[250; 240]$. The environment profile is shown in Fig. 8a and can be expressed as

$$x = 15 + 0.75t$$
$$y = 15 + 0.75t$$

Using the proposed control scheme, the force error converged to zero as shown in Fig. 8b. As previous case, force-error-overshoots are observed at transition of environmental stiffness.

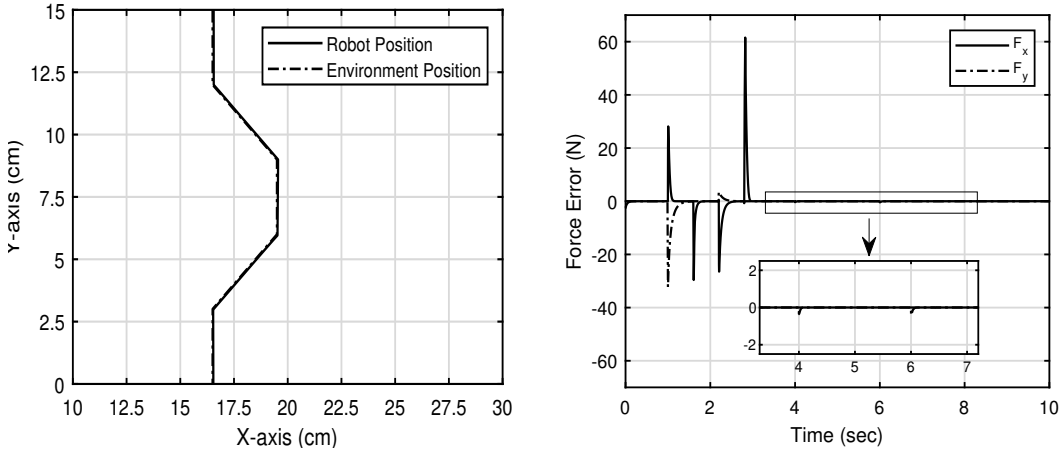

(a) Position tracking (b) Force tracking error

Fig. 9. Position and force tracking on on flat Surface with sharp edges crack using **adaptive variable impedance control**: The overshoots indicate the force error at each edge of the corner. The boxed-graph presents a very small overshoots due to variation of stiffness.

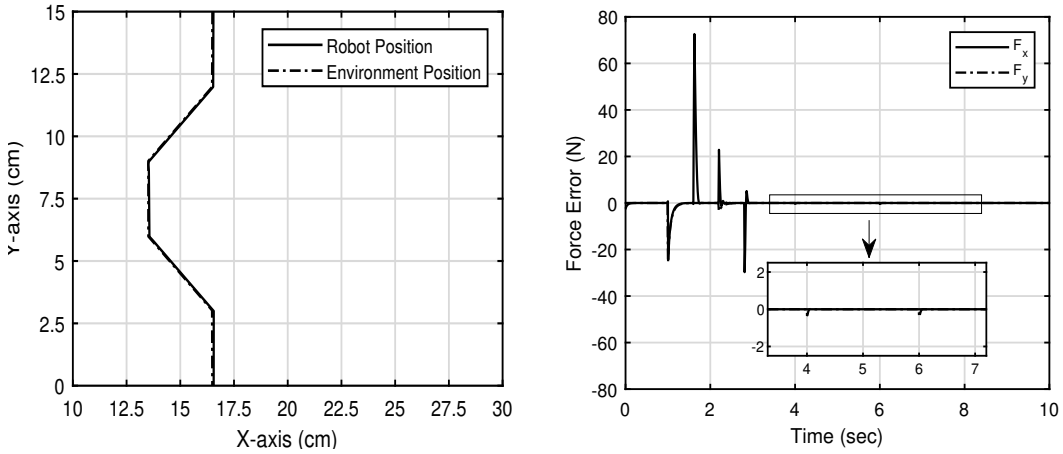

(a) Position tracking (b) Force tracking error

Fig. 10. Position and force tracking on on flat Surface with sharp edges crack using **adaptive variable impedance control**

4.3 Force Tracking on Flat Surface with Sharp Edges Crack

To observe the validity of proposed control scheme against the uneven surface, environment profile with sharp edges crack is considered as shown in Fig. 9a. The damping gains along both axes are initialized as $B = diag[310; 310]$ and the constant mass matrix as $M = diag[1; 1]$. The environment stiffness is varied according to the following profile

$$K_e = \begin{cases} 7000\ (N/m), & 0 \leq t < 4 \\ 6000\ (N/m), & 4 \leq t < 6 \\ 5000\ (N/m), & 6 \leq t \leq 10 \end{cases}$$

During time interval $1 - 3$ *sec*, the force-error-overshoots represent the force error at each corner of the crack as shown in Fig. 9b. The remaining two small spikes at $t = 4$ *sec* and $t = 6$ *sec* are due to the variation in the environment stiffness.

In addition, the extra DOF is used for avoiding the robot from a singular configuration during force tracking. The manipulability measure technique is adopted to represent the manipulability ellipsoid. Two cases are considered to differentiate the effect of the singularity avoidance algorithm: 1) DLS method 2) DLS + Singularity Avoidance. Numerical data at specific intervals can be examined in table 1. The data shows that the manipulability index improves for case 2.

4.4 Force Tracking on Flat Surface with Burr

During drilling or cutting operation, a rough projection left on a metal surface. Environment profile with sharp edges is assumed as shown in Fig. 10a. The proposed control scheme is implemented to perform force tracking on a surface with a burr. The inertia matrix M is kept constant to $diag[1; 1]$, whereas, the damping gains along both

Fig. 11. Hardware setup of 3R planar robot: The encoded Maxon drive system is controlled with myRio-1900 controller to implement the control scheme.

axes are initialized from $diag[290; 280]$. The environment stiffness is varied according to the following profile

$$K_e = \begin{cases} 7000\ (N/m), & 0 \leq t < 4 \\ 6000\ (N/m), & 4 \leq t < 6 \\ 5000\ (N/m), & 6 \leq t \leq 10 \end{cases}$$

The steady-state force error is converged to zero along both axes as shown in Fig. 10b. During time interval $1 - 3$ *sec*, the spikes represent the force error at each corner of burr.

The experimental setup is shown in a Fig. 11. Currently, the position and velocity control are implemented using myRio-1900 controller. Moreover, the authors have been working on it to implement the adaptive variable impedance control to investigate it effectiveness practically. The setup has been arranged for observing the force tracking performance in uncertain environment stiffness as well.

5. CONCLUSION

The adaptive variable impedance control scheme devised herein effectively performed force tracking on various uncertain surfaces with minor force-error-overshoot during environmental stiffness transition. The force-error-overshoot during the transition of the environment stiffness is reduced up to **56.13%** as compared to the constant impedance paradigm. Moreover, the singularity avoidance algorithm, devised by authors for redundant manipulators, improved the manipulability index by **5.95%**. This enables the robots to dynamically control force-tracking, in multiple axis; thus, executing motion over complex trajectories. The stability analysis of the proposed approach is performed using the Routh-Hurwitz criterion to figure out the controller stability region. The inverse kinematics of the 3R planar manipulator is calculated using Damped Least Square method along with the singularity avoidance algorithm. In order to ensure the performance on actual hardware, motor parameters, I/O descriptions, and the servo control scheme have been presented. Currently, the authors have been working on hardware implementation to ensure the real-time performance of the proposed scheme.

REFERENCES

Abu-dakka, F.J., Rozo, L., and Caldwell, D.G. (2018). Force-based variable impedance learning for robotic manipulation. *Robotics and Autonomous Systems*, 109, 156–167. doi:10.1016/j.robot.2018.07.008. URL `https://doi.org/10.1016/j.robot.2018.07.008`.

Albert, A. (1972). Regression and the Moore-Penrose Pseudoinverse. *Press, New York-London*.

Ba, K.x., Ma, G.l., Yu, B., Jin, Z.g., Huang, Z.p., Zhang, J.x., and Kong, X.d. (2020). A nonlinear model-based variable impedance parameters control for position-based impedance control system of hydraulic drive unit. *International Journal of Control, Automation and Systems*, 18(7), 1806–1817.

Buchli, J., Stulp, F., Theodorou, E., and Schaal, S. (2011). Learning variable impedance control. *International Journal of Robotics Research*, 30(7), 820–833. doi:10.1177/0278364911402527.

Calinon, S., Sardellitti, I., and Caldwell, D.G. (2010). Learning-based control strategy for safe human-robot interaction exploiting task and robot redundancies. *IEEE/RSJ 2010 International Conference on Intelligent Robots and Systems, IROS 2010 - Conference Proceedings*, 249–254. doi:10.1109/IROS.2010.5648931.

Chiaverini, S., Egeland, O., and Kanestrom, R. (1991). Achieving user-defined accuracy with damped least-squares inverse kinematics. In *Fifth International Conference on Advanced Robotics' Robots in Unstructured Environments*, 672–677. IEEE.

Craig, J.J. (1981). Hybrid Position / Force Control of Manipulators. *Journal of Dynamic Systems, Measurement, and Control*, 102(June 1981).

Deng, Z., Jin, H., Hu, Y., He, Y., Zhang, P., Tian, W., and Zhang, J. (2016). Fuzzy force control and state detection in vertebral lamina milling. *Mechatronics*, 35, 1–10. doi:10.1016/j.mechatronics.2016.02.004.

Ficuciello, F., Villani, L., and Siciliano, B. (2015). Variable Impedance Control of Redundant Manipulators for Intuitive Human-Robot Physical Interaction. *IEEE Transactions on Robotics*, 31(4), 850–863. doi:10.1109/TRO.2015.2430053.

Hogan, N. (1985). Impedance Control : An Approach to Manipulation : Part II — Implementation. *Journal of Dynamic Systems, Measurement, and Control*, 107(June 1983).

Jinjun, D., Yahui, G., Ming, C., and Xianzhong, D. (2018). Adaptive variable impedance control for dynamic contact force tracking in uncertain environment. *Robotics and Autonomous Systems*, 102, 54–65. doi:10.1016/j.robot.2018.01.009. URL `https://doi.org/10.1016/j.robot.2018.01.009`.

Jung, S. and Hsia, T.C. (2000). Robust neural force control scheme under uncertainties in robot dynamics and unknown environment. *IEEE Transactions on Industrial Electronics*, 47(2), 403–412. doi:10.1109/41.836356.

Jung, S., Hsia, T.C., and Bonitz, R.G. (2001). Force Tracking Impedance Control for Robot Manipulators with an Unknown Environment: Theory, Simulation, and Experiment Abstract. *The International Journal of Robotics Research*, 20, 765–774. doi:10.1177/02783640122067651.

Jung, S., Hsia, T.C., and Bonitz, R.G. (2004). Force Tracking Impedance Control of Robot Manipulators Under

Unknown Environment. *IEEE TRANSACTIONS ON CONTROL SYSTEMS TECHNOLOGY*, 12(3), 474–483.

Kiguchi, K. and Fukuda, T. (2000). Position/force control of robot manipulators for geometrically unknown objects using fuzzy neural networks. *IEEE Transactions on Industrial Electronics*, 47(3), 641–649. doi:10.1109/41.847905.

Kronander, K. and Billard, A. (2012). Online learning of varying stiffness through physical human-robot interaction. *Proceedings - IEEE International Conference on Robotics and Automation*, 1842–1849. doi:10.1109/ICRA.2012.6224877.

Kronander, K. and Billard, A. (2016). Stability Considerations for Variable Impedance Control. *Neurological Sciences*, 25. doi:10.1007/s10072-004-0214-7.

Lu, W. and Meng, Q. (1991). Impedance Control with Adaptation for Robotic Manipulations. *IEEE Transactions on Robotics AND Automation*, 7, 408–415.

Maciejewski, A.A. and Klein, C.A. (1985). Obstacle avoidance for kinematically redundant manipulators in dynamically varying environments. *The international journal of robotics research*, 4(3), 109–117.

Roy, N., Newman, P., and Srinivasa, S. (2013). Tendon-Driven Variable Impedance Control Using Reinforcement Learning. In *Robotics: Science and Systems VIII*, 369–376. MITP. URL `http://ieeexplore.ieee.org/document/6577948`.

Seraji, H. (1997). Force Tracking in Impedance Control. *International Journal of Robotics Research*, 16, No.1, 97–117.

Siciliano, B. and Villani, L. (2000). *Robot Force Control*, volume 540. Springer. doi:10.1007/978-1-4615-4431-9324.004.

Spong, M.W., Hutchinson, S., and Vidyasagar, M. (2004). *Robot Modeling and Control*. Wiley.

Wampler, C.W. (1986). Manipulator Inverse Kinematic Solutions Based on Vector Formulations and Damped Least-Squares Methods. *IEEE Transactions on Systems, Man and Cybernetics*, 16(1), 93–101. doi:10.1109/TSMC.1986.289285.

Wan, J., Yao, J., Zhang, L., and Wu, H. (2018). A weighted gradient projection method for inverse kinematics of redundant manipulators considering multiple performance Criteria. *Journal of Mechanical Engineering*, 64(7-8), 475–487. doi:10.5545/sv-jme.2017.5182.

Wang, L., Chen, Z., Chalasani, P., Pile, J., Kazanzides, P., Taylor, R.H., and Simaan, N. (2016). Updating virtual fixtures from exploration data in force-controlled model-based telemanipulation. *Proceedings of the ASME Design Engineering Technical Conference*, 5A-2016, 1–10. doi:10.1115/DETC2016-59305.

Xianjun, S. and Xi, Z. (2018). Fuzzy adaptive hybrid impedance control for mirror milling system. *Elsevier*, 53(June), 20–27. doi:10.1016/j.mechatronics.2018.05.008.

Yahya, S., Moghavvemi, M., and Mohamed, H.A. (2012). Singularity avoidance of a six degree of freedom three dimensional redundant planar manipulator. *Computers & Mathematics with Applications*, 64(5), 856–868.

Yoshikawa, T. (1984). Analysys and control of robot manipulators with redundancy. robotic research. *The First International Syposium, 1984*, 735–747.

Yoshikawa, T. (1985). Manipulability of Robotic Mechanisms. *International Journal of Robotics Research*, 4(2), 3–9. doi:10.1177/027836498500400201.

Zhang, X. and Khamesee, M.B. (2017). Adaptive Force Tracking Control of a Magnetically Navigated Microrobot in Uncertain Environment. *IEEE/ASME Transactions on Mechatronics*, 22(4), 1644–1651. doi:10.1109/TMECH.2017.2705523.